Journal of Materials Chemistry C

COMMUNICATION

View Article Online
View Journal | View Issue



Cite this: J. Mater. Chem. C, 2018, 6, 3573

Received 20th October 2017,
Accepted 13th November 2017

DOI: 10.1039/c7tc04798c

rsc.li/materials-c

# Synthesis, crystal structure, magnetic and electronic properties of the caesium-based transition metal halide $Cs_3Fe_2Br_9$†

Fengxia Wei, [ab] Federico Brivio, [a] Yue Wu, [a] Shijing Sun,[a] Paul D. Bristowe *[a] and Anthony K. Cheetham *[a]

**The diversity of halide materials related to important solar energy systems such as $CsPbX_3$ (X = Cl, Br, I) is explored by introducing the transition metal element Fe. In particular a new compound, $Cs_3Fe_2Br_9$ (space group $P6_3/mmc$ with $a$ = 7.5427(8) and $c$ = 18.5849(13) Å), has been synthesized and found to contain 0D face-sharing $Fe_2Br_9$ octahedral dimers. Unlike its isomorph, $Cs_3Bi_2I_9$, it is black in color, has a low optical bandgap of 1.65 eV and exhibits antiferromagnetic behavior below $T_N$ = 13 K. Density functional theory calculations shed further light on these properties and also predict that the material should have anisotropic transport characteristics.**



## 1. Introduction

In the past few years, lead halide perovskites such as $APbI_3$ (A = methylammonium, MA, and cesium) have attracted much attention as photovoltaic materials because of their remarkable photo-conversion efficiency in solar cell devices.[1,2] Due to the toxicity of lead and the intrinsic moisture sensitivity of the lead(II) compounds, a search for environmentally friendly alternatives has been undertaken.[3] Several perovskite-related families have been proposed, such as double perovskites where $Pb^{2+}$ is replaced by isoelectronic $Bi/In/Sb^{3+}$ and a monovalent cation, *e.g.* $(MA)_2KBiCl_6$, $(MA)_2TlBiBr_6$, $(MA)_2AgBiBr_6$ and the inorganic phases $Cs_2AgBX_6$ (X = Cl, Br and B = Bi, In).[4–11] Another popular candidate family is $A_3M_2I_9$, where A = $K^+$, $Rb^+$, $NH_4^+$, $MA^+$, $Cs^+$ *etc.*, M = $Bi^{3+}$ and $Sb^{3+}$, consisting of either corner- and edge-sharing $MI_6$ octahedral layers or face-sharing $MI_6$ dimers.[12–16] All of the above systems exhibit very interesting optoelectronic properties.

Transition metals have attracted our attention as a method of tuning the optoelectronic properties. For example, using $Fe^{3+}$ to replace $Bi^{3+}$ can reduce the bandgap: $Cs_2NaFeCl_6$, which adopts a double perovskite architecture (Fig. S1, ESI†) is red, while its Cl analogues with other trivalent cations show much lighter colours. For instance, $Cs_2NaBiCl_6$ is yellow[17] while the $Cs_2NaLnCl_6$ (Ln = Lanthanide) phases are mostly white.[18] A much darker color is expected for the hypothetical $Cs_2NaFeBr_6$, but our attempts to synthesize this compound yielded black octahedral crystals of composition $Cs_2FeBr_5{\cdot}H_2O$ (Fig. S2, ESI†), crystallizing in space group *Pnma*. This material consists of 0D $FeBr_5O$ octahedral monomers in which the oxygen is part of a water molecule, as in the known $Cs_2FeCl_5{\cdot}H_2O$.[19] The dimensionality indicates the degree of connectivity of the octahedra. In this case the octahedra are discrete.

Incorporating Fe into the $A_3Bi_2X_9$ (X = Cl, Br and I) family turns out to have a long history. $Cs_3Fe_2Cl_9$, which is dark red in color, was reported to form two polymorphs: a 2D layered system with $P\bar{3}m1$ symmetry and 0D dimeric system in space group $P6_3/mmc$,[20,21] In the latter, both intradimer and interdimer magnetic interactions are present, and the two competing interactions lead to very interesting magnetic properties. In the present work, we report a new compound, $Cs_3Fe_2Br_9$ (CCDC 1575068), which is isostructural with $Cs_3Bi_2I_9$ (red)[13] and $(MA)_3Bi_2I_9$ (red),[14] yet is black in color. Its variable temperature behavior, thermal stability, optical and magnetic properties are investigated in combination with density functional theory (DFT) calculations.

## 2. Experimental and computational methods and results

### 2.1 Synthesis

A two-step synthesis method was used, involving both hydrothermal and room temperature crystallization. 2 mmol CsBr (99.9%, Sigma Aldrich), 1 mmol $FeCl_3{\cdot}6H_2O$ (>99%, Sigma Aldrich) together with 1.5 ml HBr acid (47 wt%) were placed in

[a] Department of Materials Science and Metallurgy, University of Cambridge, CB3 0FS, UK. E-mail: akc30@cam.ac.uk, pdb1000@cam.ac.uk
[b] Institute of Materials Research and Engineering, Agency for Science, Technology and Research, 2 Fusionopolis Way, Singapore

† Electronic supplementary information (ESI) available: Additional information, including CIF files, experimental methods and further information on the DFT calculations. CCDC 1575067–1575070. For ESI and crystallographic data in CIF or other electronic format see DOI: 10.1039/c7tc04798c

a 23 ml stainless steel Parr autoclave and heated at 160 °C for 3 days. Intermediate products of brown needle shaped crystals of $CsFeBr_4$ (Fig. S3, ESI†) were formed. The Teflon autoclave was then left in the fume hood at room temperature (>15 °C) and black crystals formed after one week. The following chemical reactions take place during the synthesis:

$$CsBr + FeCl_3{\cdot}6H_2O + 3HBr \rightarrow CsFeBr_4 + 3HCl + 6H_2O \quad (1)$$

$$CsBr + 2CsFeBr_4 \rightarrow Cs_3Fe_2Br_9 \quad (2)$$

During the hydrothermal process, reaction (1) dominates and almost no black $Cs_3Fe_2Br_9$ is formed. Even using exact stoichiometric ratios of the starting reagents does not result in the target material. However, black octahedral crystals of $Cs_3Fe_2Br_9$, ~0.5 mm in size, can be collected after standing at room temperature for 3 weeks. The sample is soluble in most polar solvents, including water, ethanol and acetone.

### 2.2 Crystallographic studies

$Cs_3Fe_2Br_9$ crystallizes in the hexagonal space group $P6_3/mmc$ ($a$ = 7.5427(8) and $c$ = 18.5849(13) Å). It consists of face-sharing $Fe_2Br_9$ octahedral dimers with Cs serving as bridging atoms between the dimers (Fig. 1a and b). The octahedra are slightly distorted, with two sets of Fe–Br bonds (2.427(1) Å and 2.701(2) Å) and distorted Br–Fe–Br angles (80.76(6)°, 90.55(3)° and 97.01(7)°), compared to the nominal octahedral angle of 90°. Due to the Coulombic repulsive force between the cations within the dimer (Fe–Fe distance = 3.585(3) Å), the $Fe^{3+}$ ions are displaced outwards with respect to the shared face. Therefore, the smallest octahedral angles and longer Fe–Br bonds are found with the shared $Br^-$ ions (Fig. 1) and the largest angles and shorter Fe–Br distances are from the unshared ones. According to the interatomic distances, the bond strengths between $Fe^{3+}$ and unshared $Br^-$ are stronger than those with shared $Br^-$ ions. Moreover, the angular distortion of the $Br_{shared}$–Fe–$Br_{unshared}$ angle is minor (90.55°). The shortest distance between Cs and Br is 3.762(1) Å.

Variable temperature single crystal diffraction suggests no phase transition down to 120 K. The thermal expansion coefficients are approximately linear with $\alpha_a$ = 45.3 $MK^{-1}$, $\alpha_c$ = 39.6 $MK^{-1}$, giving $\alpha_v$ = 131.2 $MK^{-1}$. The repulsion between the $Fe^{3+}$ ions in the dimeric unit decreases upon cooling, as shown by the less distorted octahedral dimer and reduced interatomic Fe···Fe distances (Fig. S4, ESI†). As a result, negative expansion occurs for the shorter bonds and positive thermal expansion is found for the longer bonds. A similar phenomenon is observed for the octahedral angles: on cooling, the smaller angles tend to increase, while the larger angles decrease.

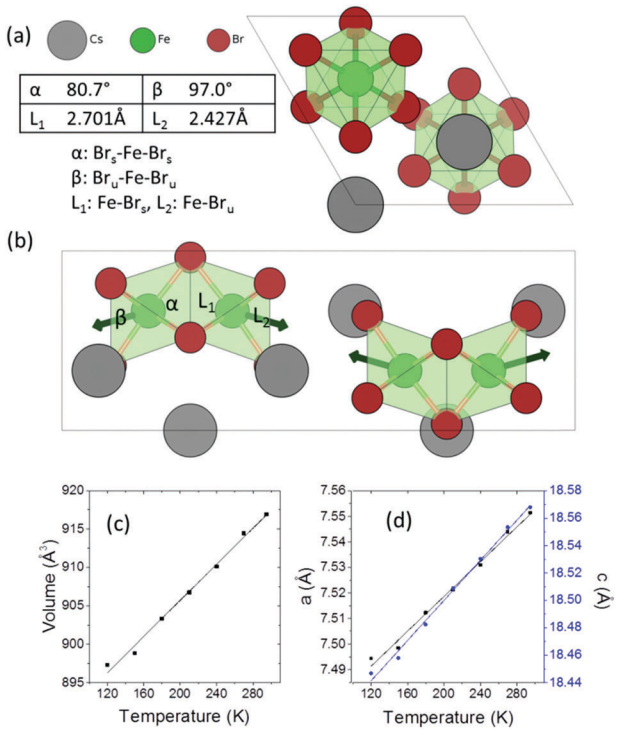


Fig. 1 (a) Crystal structure of $Cs_3Fe_2Br_9$ viewed along the $c$-axis, (b) view along the $b$-axis showing of the $Fe_2Br_9$ dimers. The angles and bond lengths illustrate the distortion of the octahedra. The subscripts s and u indicate shared and unshared Br anions respectively and the arrows indicate the direction of Coulombic repulsion between cations, (c) cell volume and (d) lattice parameters as a function of temperature measured using single crystal X-ray diffraction.

### 2.3 Thermal analysis

Thermal stability was investigated using an SDT (simultaneous differential scanning calorimetry (DSC) – thermogravimetric analysis (TGA)) Q600 instrument. Powder samples were heated from room temperature to 1123 K at 10 K $min^{-1}$ under an air flow of 100 ml $min^{-1}$. $Cs_3Fe_2Br_9$ is stable until 537.5 K and then experiences a two-step decomposition process (Fig. 2). When the sample is heated, moisture and residual HBr at the particle surfaces start to evaporate, resulting in a small weight loss (~3.6%) at the beginning of the curve. For comparison, the thermal stability of its bismuth analogues $Cs_3Bi_2I_9$ and $MA_3Bi_2I_9$ were also measured; the former decomposed at 636.4 K, while the latter was stable until 529.3 K (Fig. S5 and S6, ESI†).

### 2.4 Optical characterization

The optical bandgap was measured on a PerkinElmer Lambda 750 UV-Visible spectrometer in the absorption mode with a

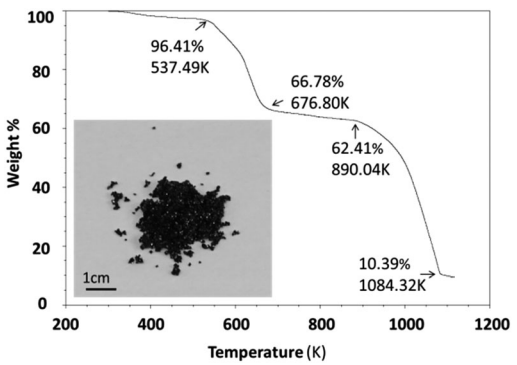


Fig. 2 Thermogravimetric analysis curve; the inset shows a photo of the sample (small crystals).

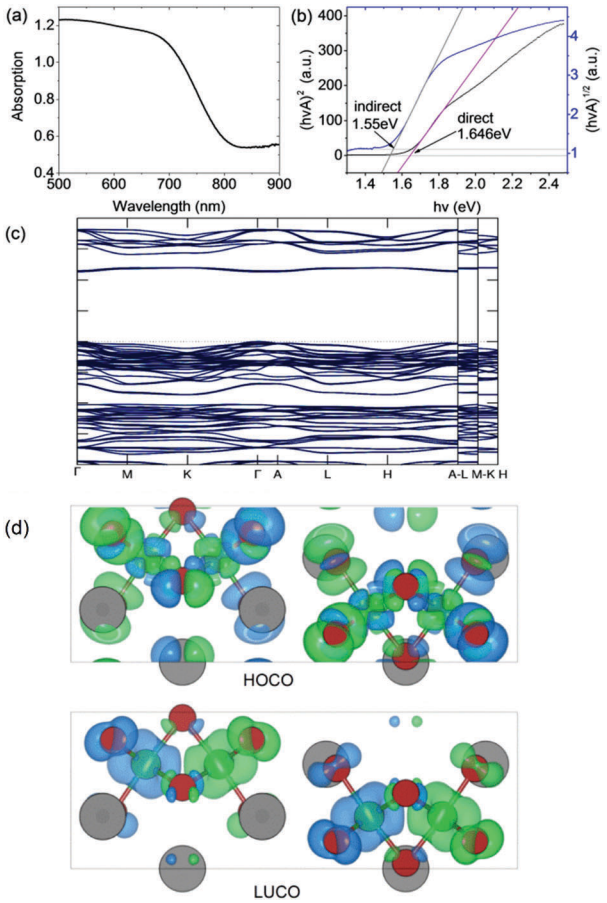


Fig. 3 (a) Absorption spectrum and (b) Tauc plot for indirect and direct bandgaps. (c) Band structure (non-magnetic case) calculated using the HSE06 exchange–correlation functional. (d) Charge density isosurfaces (antiferromagnetic case) calculated using the PBEsol exchange–correlation functional and viewed along the *b*-axis. The top and bottom panels show the Highest Occupied Crystal Orbital (HOCO) and Lowest Unoccupied Crystal Orbital (LUCO) respectively. The charge is displayed using a threshold of 0.001 e $Bohr^{-3}$. The different spin channels are shown in blue and green. Atom colors are the same as in Fig. 1.

2 nm slit width. The scan interval was 1 nm and the scan range was between 500 and 1100 nm. The absorption edge is observed at ~800 nm (*i.e.* 1.55 eV). In accordance with our DFT calculation (see below), we deduced a direct optical bandgap of ~1.65 eV from the Tauc plot derived from the reflectance spectrum (Fig. 3). Note that the analogous $A_3Bi_2I_9$ phases (A = Cs and MA) were reported to have indirect bandgaps which are larger in the range 1.9 eV to 2.2 eV.[22,23]

### 2.5 Density functional calculations

The DFT calculations were performed using the projector augmented wave (PAW) method as implemented in VASP.[24] The experimental structure obtained at room temperature was fully optimized using the PBEsol exchange–correlation functional[25] which reduced the atomic forces below 1 meV $Å^{-1}$ at effectively zero Kelvin (see ESI† for further computational details). The resulting atomic positions are given in Table S1 (ESI†). The presence of Fe in the material suggests that it could exhibit magnetic ordering due to unpaired 3d electrons. To examine this possibility, spin-polarized calculations were performed on the optimized structure in the ferromagnetic (FM) state and three possible antiferromagnetic (AFM) states. It was found that one of the AFM states in which neighboring Fe atoms have opposite spin orientation is significantly lower in energy than either the FM or non-magnetic states, by 80 meV $f.u.^{-1}$ and 335 meV $f.u.^{-1}$ respectively (see Table S2 (ESI†) for details). The calculations therefore predict that at very low temperatures $Cs_3Fe_2Br_9$ prefers to be antiferromagnetic. The calculated magnetic moment on each Fe atom is 3.38 $\mu_B$. This value is lower than the value of 5.79 $\mu_B$ obtained from analysis of the magnetic susceptibility data in the higher temperature paramagnetic region (see below). There are several reasons for this, including the well-known reduction in spin in magnetically ordered structures due to covalency. For example, neutron scattering measurements on $FeCl_3$ show that the spin is reduced to 4.7(3) $\mu_B$ in the antiferromagnetic phase.[26] Fig. 3 shows charge density isosurfaces corresponding to the HOCO and LUCO for the lowest energy AFM state.

Table 1 Calculated effective masses (relative to the rest mass $m_0$)

| | $\Gamma \rightarrow M$ | $\Gamma \rightarrow K$ | $\Gamma \rightarrow A$ |
|---|---|---|---|
| $m_h^*/m_o$ | −0.11 | −0.06 | −1.02 |
| $m_e^*/m_o$ | 0.25 | 0.16 | 13.87 |

In order to determine an improved band structure for $Cs_3Fe_2Br_9$ the HSE06 hybrid exchange–correlation functional was used,[27] although it is acknowledged that GW would normally be the preferred method. The calculation was performed on the non-magnetic state to contain the cost of the calculation and because previous work has indicated that, while HSE06 provides a reasonable band structure, it may not be adequate for magnetic properties.[28] The material is found to have a 2.254 eV direct band gap which occurs at the $\Gamma$ point with a relatively flat band structure (Fig. 3). At the band edge it is possible to calculate the effective masses in the parabolic approximation (Table 1). The values indicate a high anisotropy with reduced transport along the *c*-direction ($\Gamma \rightarrow A$). The Fe atoms have been described with $3p^6 3d^7 4s^1$ as valence electrons, while other core states have been substituted by the pseudopotential. The valence band maximum (VBM) contains Fe 3d and Br 4p states, whereas the conduction band minimum (CBM) contains mostly Fe 3d, Fe 4s and Br 4p states.

### 2.6 Magnetic measurements

Magnetic susceptibility measurements, $\chi(T) = M(T)/H$, were conducted using a Quantum Design Magnetic Properties Measurement System (MPMS3) with a superconducting interference device (SQUID) magnetometer. Measurements were made after cooling in zero field (ZFC) and in a measuring field (FC) of $\mu_0 H = 0.01$ T over the temperature range $2 \leq T \leq 300$ K. $Cs_3Fe_2Br_9$ shows antiferromagnetic behavior with a Néel temperature $T_N$ = 13 K (Fig. 4), higher than that of analogous $Cs_3Fe_2Cl_9$ which also exhibits an antiferromagnetic long range order at $T_N$ = 5.3 K.[29] The results are in good agreement with the DFT calculations.

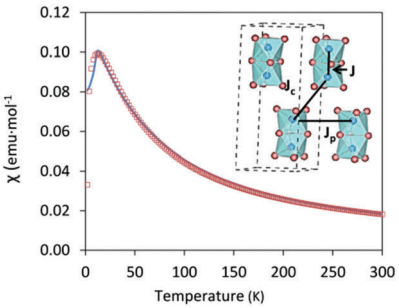


Fig. 4 Magnetic susceptibility as a function of temperature, blue: experimental, red square: fitted curve using dimer model. The inset illustrates the definition of $J$, $J_p$ and $J_c$. Cs atoms are not included for clarity.

Appling the Curie–Weiss law in the paramagnetic region (from 50 K to 300 K), a negative Weiss constant of −36.10(3) K was obtained, as expected for an antiferromagnetic compound (Fig. S7, ESI†) and the calculated effective magnetic moment $\mu_{eff}$ was 5.79(4) $\mu_B$. In order to obtain a comprehensive $\chi$ fitting from 2 K to 300 K, a weakly coupled dimer model was applied (see ESI† for fitting formula).[30] This system contains $Fe^{3+}$ ions as dimeric units $Fe_2Br_9$, with three distinct Fe–Fe distances (3.585(3), 7.179(2) and 7.543(1) Å) corresponding to intradimer ($J$) and interdimer ($J_c + J_p$) interactions, respectively. The dominant intradimer exchange yields $J = -8.2$ K, while the weak interdimer interactions between the $Fe^{3+}$ of neighbouring dimers are given as $J_p + J_c = -3.4$ K. The intradimer interactions are weaker than those in the Cr counterpart, $Cs_3Cr_2Br_9$, which was reported to have $J = -10.3$ K, corresponding to a shorter Cr–Cr distance ~3.317(4) Å. On the other hand, the interdimer interactions of $Cs_3Cr_2Br_9$ are weaker with $J_p + J_c = -1.1$ K due to the longer distances (7.420(1) and 7.507(1) Å).[30] In the case of $Cs_3Fe_2Cl_9$, both intra- and interdimer interactions are smaller ($J = -2.4$ K and $J_p + J_c = -1.2$ K for single crystals).[29]

## 3. Conclusions

We have synthesized black crystals of $Cs_3Fe_2Br_9$ and determined its crystal structure. $Cs_3Fe_2Br_9$ crystallizes in the hexagonal space group $P6_3/mmc$ and the structure contains $Fe_2Br_9$ face-sharing octahedral dimers. The Fe–Br bond strengths differ between the shared and unshared faces, and the distorted octahedra tend to become more symmetrical upon cooling due to the reduced cation–cation Coulombic repulsion. The compound is thermally stable up to 537.5 K, and has an optical bandgap of 1.65 eV. DFT calculations indicate that the band gap is direct and also predict reduced transport along the $c$-direction. Magnetic susceptibility measurements show antiferromagnetic behavior, with $T_N = 13$ K, and can be fitted with a weakly coupled dimer model. The spin polarized DFT calculations agree with this behavior at low temperatures and predict which antiferromagnetic configuration is preferred.

## Conflicts of interest

There are no conflicts to declare.

## Acknowledgements

F. Wei is a holder of an A*STAR international fellowship granted by the Agency for Science, Technology and Research, Singapore. A. K. Cheetham and Y. Wu thank the Ras al Khaimah Center for Advanced Materials for financial support. The calculations were performed at the Cambridge HPCS and the UK National Supercomputing Service, ARCHER. Access to the latter was obtained *via* the Materials Chemistry Consortium and funded by EPSRC under Grant Number EP/L000202/1.

## Notes and references

1 A. Kojima, K. Teshima, Y. Shirai and T. Miyasaka, *J. Am. Chem. Soc.*, 2009, **131**, 6050–6051.
2 M. M. Lee, J. Teuscher, T. Miyasaka, T. N. Murakami and H. J. Snaith, *Science*, 2012, **338**, 643–647.
3 W. Li, Z. Wang, F. Deschler, S. Gao, R. H. Friend and A. K. Cheetham, *Nat. Rev. Mater.*, 2017, **2**, 16099.
4 F. Wei, Z. Deng, S. Sun, F. Xie, G. Kieslich, D. M. Evans, M. A. Carpenter, P. D. Bristowe and A. K. Cheetham, *Mater. Horiz.*, 2016, **3**, 328–332.
5 F. Wei, Z. Deng, S. Sun, F. Zhang, D. M. Evans, G. Kieslich, S. Tominaka, M. A. Carpenter, J. Zhang, P. D. Bristowe and A. K. Cheetham, *Chem. Mater.*, 2017, **29**, 1089–1094.
6 Z. Deng, F. Wei, S. Sun, G. Kieslich, A. K. Cheetham and P. D. Bristowe, *J. Mater. Chem. A*, 2016, **4**, 12025–12029.
7 A. H. Slavney, L. Leppert, D. Bartesaghi, A. Gold-Parker, M. F. Toney, T. J. Savenije, J. B. Neaton and H. I. Karunadasa, *J. Am. Chem. Soc.*, 2017, **139**, 5015–5018.
8 A. H. Slavney, T. Hu, A. M. Lindenberg and H. I. Karunadasa, *J. Am. Chem. Soc.*, 2016, **138**, 2138–2141.
9 G. Volonakis, A. A. Haghighirad, R. L. Milot, W. H. Sio, M. R. Filip, B. Wenger, M. B. Johnston, L. M. Herz, H. J. Snaith and F. Giustino, *J. Phys. Chem. Lett.*, 2017, **8**, 772–778.
10 G. Volonakis, M. R. Filip, A. A. Haghighirad, N. Sakai, B. Wenger, H. J. Snaith and F. Giustino, *J. Phys. Chem. Lett.*, 2016, **7**, 1254–1259.
11 E. T. McClure, M. R. Ball, W. Windl and P. M. Woodward, *Chem. Mater.*, 2016, **28**, 1348–1354.
12 S. Sun, S. Tominaka, J.-H. Lee, F. Xie, P. D. Bristowe and A. K. Cheetham, *APL Mater.*, 2016, **4**, 31101.
13 B. Chabot and E. Parthe, *Acta Crystallogr., Sect. B: Struct. Crystallogr. Cryst. Chem.*, 1978, **34**, 645–648.
14 R. Jakubas, J. Zaleski and L. Sobczyk, *Ferroelectrics*, 1990, **108**, 109–114.
15 A. J. Lehner, D. H. Fabini, H. A. Evans, C.-A. Hébert, S. R. Smock, J. Hu, H. Wang, J. W. Zwanziger, M. L. Chabinyc and R. Seshadri, *Chem. Mater.*, 2015, **27**, 7137–7148.
16 B. Saparov, F. Hong, J.-P. Sun, H.-S. Duan, W. Meng, S. Cameron, I. G. Hill, Y. Yan and D. B. Mitzi, *Chem. Mater.*, 2015, **27**, 5622–5632.
17 L. R. Morss, M. Siegal, L. Stenger and N. Edelstein, *Inorg. Chem.*, 1970, **9**, 1771–1775.
18 G. Meyer, *Prog. Solid State Chem.*, 1982, **14**, 141–219.

19 C. J. O'Connor, B. S. Deaver and E. Sinn, *J. Chem. Phys.*, 1979, **70**, 5161–5167.
20 H. Yamatera and K. Nakatsu, *Bull. Chem. Soc. Jpn.*, 1954, **27**, 244.
21 M. T. Kovsarnechan, J. Roziere and D. Mascherpa-Corral, *J. Inorg. Nucl. Chem.*, 1978, **40**, 2009–2011.
22 B. W. Park, B. Philippe, X. Zhang, H. Rensmo, G. Boschloo and E. M. J. Johansson, *Adv. Mater.*, 2015, **27**, 6806–6813.
23 A. J. Lehner, D. H. Fabini, H. A. Evans, C. A. Hébert, S. R. Smock, J. Hu, H. Wang, J. W. Zwanziger, M. L. Chabinyc and R. Seshadri, *Chem. Mater.*, 2015, **27**, 7137–7148.
24 G. Kresse, *Phys. Rev. B: Condens. Matter Mater. Phys.*, 1999, **59**, 1758–1775.
25 J. P. Perdew, A. Ruzsinszky, G. I. Csonka, O. A. Vydrov, G. E. Scuseria, L. A. Constantin, X. Zhou and K. Burke, *Phys. Rev. Lett.*, 2008, **100**, 136406.
26 J. W. Cable, M. K. Wilkinson, E. O. Wollan and W. C. Koehler, *Phys. Rev.*, 1962, **127**, 714–717.
27 A. V. Krukau, O. A. Vydrov, A. F. Izmaylov and G. E. Scuseria, *J. Chem. Phys.*, 2006, **125**, 224106.
28 R. Grau-Crespo, H. Wang and U. Schwingenschlögl, *Phys. Rev. B: Condens. Matter Mater. Phys.*, 2012, **86**, 081101.
29 Y. Ishii, N. Noguchi, H. Yoshida and M. Oda, *Meet. Abstr. Phys. Soc. Japan*, 2016, **71.1**, 1081.
30 B. Leuenberger, H. U. Güdel and P. Fischer, *J. Solid State Chem.*, 1986, **64**, 90–101.